Proceedings of the Twenty-eighth (2018) International Ocean and Polar Engineering Conference
Sapporo, Japan, June 10-15, 2018

ISBN 978-1-880653-87-6; ISSN 1098-6189

www.isope.org

Single blade installation using active control of three tugger lines

Zhengru Ren[1,2,3], *Zhiyu Jiang*[1,3], *Roger Skjetne*[1,2,3], *Zhen Gao*[1,2,3]
[1] Centre for Research-based Innovation of Marine Operations (SFI MOVE),
[2] Centre for Autonomous Marine Operations and Systems (AMOS),
[3] Department of Marine Technology, Norwegian University of Science and Technology (NTNU), NO-7491 Trondheim, Norway

ABSTRACT

Single blade installation using jack-up vessels is a commonly used blade installation setup for offshore wind turbines. During this operation, each blade is lifted by the main crane from the deck, moved, and then bolted to the rotor hub at the top of the turbine tower. Tugger lines from the crane boom are connected to the suspended blade to reduce the blade's pendulum motions. Lately, much research has been conducted to reduce the blade motion by actively controlling the tension force in the tugger lines. Since the tugger lines can only provide positive tension, pretension is needed before the mating process. In this paper, an active PID control strategy with a three-tugger-line configuration is proposed to reduce the blade motion by controlling the tugger line forces acting on the blade . The placement of the additional 3^{rd} line is discussed. The control allocation is achieved by convex programming with an auto-generation solver using CVXGEN. Simulations under turbulent wind conditions are conducted to verify the active control scheme in HAWC2. The results shows that the active control scheme effectively reduces the translational motion of the blade root relative to the hub in the mean wind direction.

KEY WORDS: Single blade installation; PID controller; wind turbine installation; control allocation.

INTRODUCTION

Offshore wind turbines (OWTs) have attracted increasing global attention due to advantages, such as saving land resources and a superior energy quality. However, the price of electricity from offshore wind in 2016 is still approximately 3-4 times greater than that of electricity from onshore wind. During an OWT installation, much time is spent on waiting for the allowable weather window. Hence, OWT assembly and installation are expensive, accounting for more than 10% of the OWT overall capital expenditures (Moné et al. 2017).

As the blade span exceeds 60 m, lifting an entire rotor assembly offshore may face more challenges in addition to transportation issues. Single blade installation is one of many OWT blades installation approaches, where one blade is lifted by the main crane and attached to the hub on the top of the turbine tower. The suspended blade and the crane boom are connected by tugger lines, typically without any active control. State-of-the-art single blade installation is limited to a mean-wind speed of 8-12 m/s (Gaunaa et al. 2014). The benefits of the single blade installation are a wider range of installation vessels, lower crane capacity, and higher deck usage. On the other hand, it requires a higher number of the offshore lifts.

A few publications can be found related to various aspects of the single blade installation. The aerodynamics and aeroelastic behavior of the installation scheme are studied in, for example, Gaunaa et al. (2014, 2016). The motion characteristics are identified in Zhao et al. (2018), and the critical parameters are investigated in Jiang et al. (2018). A simulation-based verification model of single blade installation, for the purpose of control design, is proposed in Ren et al. (2018*b*), and a feedback linearization controller is proposed and verified by with the simulation-based model in Ren et al. (2018*a*). Specialized commercial products, such as LT575 Blade Dragon developed by Liftra and Boom Lock technology from HighWind are developed to advance the single blade installation.

In addition to the blade motion, the motion of the foundation also influences the success rate and impact force of the blade's final mating operation (Jiang et al. 2018, Verma et al. 2017). In this paper, a monopile foundation is considered as the support structure. At present, monopiles are the most cost-effective type of support structure. A monopile foundation is exposed to the environmental load effects of current, wind, and waves. So far, the turbine hub motion becomes quite complex. The dynamics of monopile foundation is studied in Jonkman et al. (2008). In this paper, a closed-loop feedback control scheme for single blade installation, using a PID controller for the tugger line forces, is proposed.

The paper is structured as follows. The system description and problem formulation are presented in Section 2. In Section 3, system modeling is briefly introduced. Section 4 discusses the capability of four different configurations of tugger lines. Additionally, a PID controller and an online control allocation based on convex programming are proposed. In Section 5, simulations are conducted using HAWC2 coupled with a MATLAB/Simulink interface for the developed controller. Verification of the control scheme using both the simplified model and the high-fidelity model was performed. A set of comparative studies are conducted to prove the active controller performance. Section 6 presents

conclusions and recommendations for future studies.

Notation: Scalars, vectors, and matrices are denoted with normal lowercase letters, bold lowercase letters, and bold capital letters, respectively. $|x|$ and $\|x\|_{\boldsymbol{A}}$ stand for the Euclidean norm and the weighted Euclidean norm, respectively, i.e., $|x|^2 = x^\top x$ and $\|x\|_A^2 = x^\top \boldsymbol{A} x$. The bar operator, $\bar{\cdot}$, stands for the mean value over a period.

PROBLEM FORMULATION

Description of the single blade installation

The procedure of single blade installation is described as follows. The monopile, transition piece, tower, nacelle, and blades have already been assembled. Before the blade installation begins, the hub is rotated to a horizontal position. Next, the blade is equipped by a yoke at its center of mass and lifted to the hub height by the crane from the deck. The blade root motions are monitored. If the relative displacement and velocity between the blade root and hub are within the allowable limits, then the mating process follows. Figure 1 illustrates a typical mating phase between the blade and hub. Wind-induced blade motions are controlled by the tugger lines. The mating process is finished, when the guiding pins on the blade root have entered the flange holes on the hub. Then, the blade is bolted onto the hub, followed by retraction of the lifting gear. A detailed description of the procedure can be found in Jiang et al. (2018) and Ren et al. (2018*a*).

Problem statement

In reality, the blade's final installation stage may not be as smooth as described above, especially under high wind speeds. A typical single blade installation scenario is illustrated in Fig. 2. The leading edge of the blade faces downward with a $-90°$ pitch angle. This blade orientation does not have minimal loading, but it is often adopted in practice due to the concerns for transportation and loading predictability when wind direction changes (Kuijken 2015). One lift wire is used to rigidly connect the hook and crane tip, and two slings are used to connect the hook and yoke. For the sake of simplification, only horizontal restoring force components from the tugger lines are considered. A three-tugger-line configuration is proposed, i.e., three horizontal tugger lines are connected to the yoke-blade system with arm lengths of r_{t1}, r_{t2}, and r_{t3} relative to the blade center of gravity (COG). These lines help to limit the blade pendulum motions in the horizontal plane. Typical two-tugger-line installation configurations have been considered in Kuijken (2015), Zhao et al. (2018), Jiang et al. (2018), and Ren et al. (2018*a*).

The global reference frame $\{G\}$ is utilized. The origin O_g is placed at the mean water level with the x-axis pointing in the mean wind direction, the z-axis pointing downward, and the y-axis follows the right-hand rule. The rotations about the x-, y-, and z-axes are named roll (ϕ), pitch (θ), and yaw (ψ), respectively.

The gravity is balanced by the lift wire since the blade is seized at its COG. The impact of the wind-induced lift force on the blade vertical motion is very limited. Aeroelastic simulation results in Jiang et al. (2018) have illustrated that the three planar motions are critical for a single blade installation operation in a turbulent wind field, i.e., surge (x), sway (y), and yaw (ψ). The motion in the x-axis is critical because a large wind-induced force is exerted on the yoke-blade system. The wind-induced forces acting on the blade are uneven, and the blade experiences a yaw angle of ψ, as shown. Additionally, the wind-induced force in the longitude direction is quite small compared to the drag force in the mean wind direction; refer Ren et al. (2018*b*) for details. Suppose that the tugger lines are horizontally arranged with no vertical force components; then, the horizontal tension in each line can be denoted by f_1, f_2, and f_3. It is assumed that f_1, f_2, and f_3 are constant in the x-axis. The turbulent wind continuously affects the loading situation of the blade. Therefore, a 6DOF problem is transferred into a 2DOF problem for a single blade installation operation. The control objective is to control the blade COG to track the desired setpoint $\boldsymbol{r}_d = [x_d, \psi_d]^\top$ by controlling the force inputs, f_1, f_2, and f_3. The ultimate goal is to reduce the motion of the root center in order to ensure the mating operation.

Fig. 1 Illustration of the mating phase during a single blade installation (image source: Schneider (2014)).

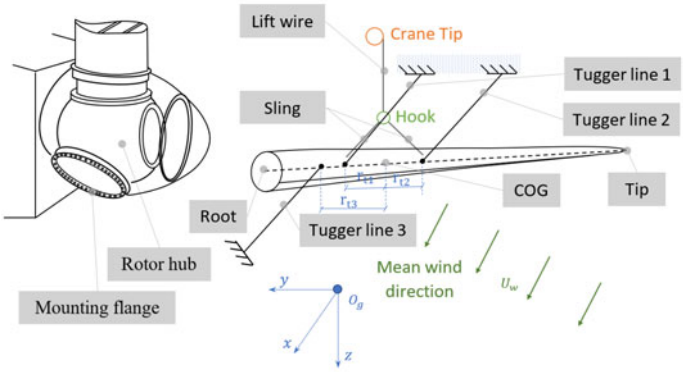

Fig. 2 Single blade installation configuration in this paper.

SYSTEM MODELING

A jack-up vessel with cranes is assumed to perform the blade installation task. The jack-up vessel and the crane are assumed to be rigid and, therefore, no external loads on them are modeled. However, the aerodynamic loads on the lifted blade and the induced blade motions are considered. Moreover, the displacements of the nacelle due to the hydrodynamic loads on the monopile are modeled.

Environment

Irregular waves were generated using the JONSWAP spectrum (DNV 2000). The hydrodynamic loads on the monopile are calculated using Morison's equation. The current velocity is assumed to be constant during the period of operation.

Mann's turbulence model is adopted to simulate the turbulent wind field (Mann 1998). The wind speed vector at a point in space is a sum of the mean-wind velocity and a turbulence. The aerodynamic load on the blade is calculated based on the cross-flow principle, i.e., an integration of the lift and drag forces along the spanwise direction. The wind load in the spanwise direction is negligible. The aerodynamic effect of dynamic stall is not considered, but static stall is inherently accounted for using the lift and drag curves of the airfoil.

Blade model

The NREL 5MW wind turbine is selected as the objective of installation.

Tugger lines

Tugger lines are modeled as springs, which only provide tension forces in the axial direction of the wire.

Monopile foundation and support structures

Various simplified models and high-fidelity simulation models for dynamic load and response analysis of monopile foundations have been investigated in earlier researches, e.g., Jonkman et al. (2008). Here, a distributed model is adopted, namely the Winkler approach, for monopile-soil interaction. The soil, modeled as plastic material, is layered with different properties, i.e., effective weight and angle of internal friction. Defined in American Petroleum Institute (2000), the soil resistance p is a function of the pile displacement y at a given point along the pile, namely, the $p-y$ model. Each layer is modeled as an uncoupled nonlinear spring with the corresponding stiffness, see Fig. 3. Timoshenko beams are used to model the pile, the transaction piece, and the tower (Bhattacharya & Adhikari 2011, Arany et al. 2016). The waves enter from 30 deg north of east.

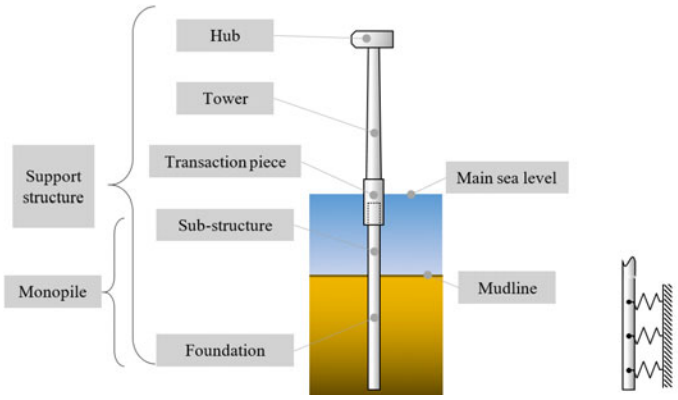

Fig. 3 OWT with monopile foundation (left) and distributed spring model (right).

CONFIGURATION OF TUGGER LINES AND CONTROL ALLOCATION

PID controller

A proportional-integral-derivative (PID) control algorithm for tugger line tension is used to stabilize the blade's motion. The control law is given by

$$\boldsymbol{\tau}_c = \begin{bmatrix} F_{tx} \\ M_{tz} \end{bmatrix} = -\boldsymbol{K}_p \begin{bmatrix} x - x_d \\ \psi - \psi_d \end{bmatrix} - \boldsymbol{K}_d \begin{bmatrix} u \\ r \end{bmatrix} - \boldsymbol{K}_i \int \begin{bmatrix} x - x_d \\ \psi - \psi_d \end{bmatrix} dt, \tag{1}$$

where F_{tx} and M_{tz} are the commanded force and torque to act on the suspended blade in the x-axis and about the z-axis, and $\boldsymbol{K}_p, \boldsymbol{K}_d, \boldsymbol{K}_i \in \mathbb{R}^{2\times 2}$ are the proportional, derivative, and integral diagonal gain matrices, respectively.

Discussion of the tugger lines configuration

As the tugger lines can only provide non-negative force inputs to the suspended blade, the control input vector $[F_{tx}, M_{tz}]^\top$ is limited by the capability of the crane and winches. In this paper, it is assumed that the placement of the first and second tugger lines follow the typical configuration with $r_{t1} = -r_{t2}$, i.e., they are assembled symmetrically on each side pf the blade COG, and both of them provide tension forces in the direction opposite to the mean-wind direction. The third tugger line is free to be placed in a range, e.g., $-10 \le r_{t3} \le 10$, and it should provide tension force in the mean-wind direction.

Suppose that the force input limits to all the tugger lines are the same. Hence, the allowable tugger line control set is

$$\mathbb{D}_f = \{f | 0 \le f \le f_{max}\},\ f_i \in \mathbb{D}_f,\ i = 1, 2, 3, \tag{2}$$

where f_{max} is the upper limit of f.

A comprehensive analysis is conducted to discuss how to configure the third tugger line. The free body diagram of a three-tugger-line configuration is shown in Fig. 4. The overall control configuration is then given by

$$\begin{aligned} \begin{bmatrix} F_{tx} \\ M_{tz} \end{bmatrix} &= \begin{bmatrix} f_1 + f_2 - f_3 \\ f_1 r_{t1} \cos\psi + f_2 r_{t2} \cos\psi - f_3 r_{t3} \cos\psi \end{bmatrix} \\ &= \begin{bmatrix} 1 & 1 & -1 \\ r_{t1}\cos\psi & r_{t2}\cos\psi & -r_{t3}\cos\psi \end{bmatrix} \begin{bmatrix} f_1 \\ f_2 \\ f_3 \end{bmatrix}. \end{aligned} \tag{3}$$

On vector form, this is written

$$\boldsymbol{\tau} = \boldsymbol{B}\boldsymbol{f}, \tag{4}$$

where $\boldsymbol{\tau} = [F_{tx}, M_{tz}]^\top \in \mathbb{R}^2$ is the commanded load vector on the blade resulting from the tugger line force vector $\boldsymbol{f} = [f_1, f_2, f_3]^\top \in \mathbb{D}_f^3$, and $\boldsymbol{B}$ is the tugger line configuration matrix. Control allocation is now the inverse problem of Eqn. (5), that is, allocating commanded forces $\boldsymbol{f}_c \in \mathbb{R}^3$ for the tugger lines given a commanded load vector $\boldsymbol{\tau}_c \in \mathbb{R}^2$, according to

$$\boldsymbol{\tau}_c = \boldsymbol{B}\boldsymbol{f}_c, \tag{5}$$

where $\boldsymbol{f}_c = [f_{c,1}, f_{c,2}, f_{c,3}]^\top$ is the control command vector.

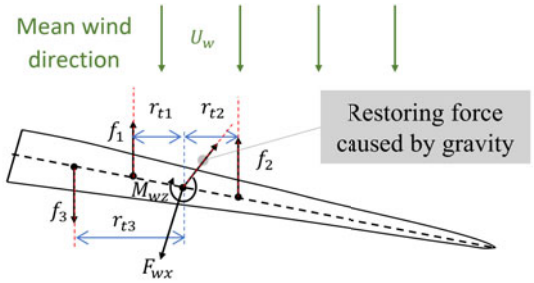

Fig. 4 Free body diagram in the horizontal.

Based on the quasi-static results of the wind-induced force in the mean wind direction and moment about z-axis for a vertically arranged blade, F_{wx} and M_{wz}, follow quadratic relations, i.e.,

$$\begin{bmatrix} F_{wx} \\ M_{wz} \end{bmatrix} = \begin{bmatrix} k_{F_x} \\ k_{M_z} \end{bmatrix} U_w^2, \tag{6}$$

where $k_{F_x} = -0.174\ kN \cdot s^2/m^2$ and $k_{M_z} = -1.474\ kN \cdot s^2/m^2$ for a NREL 5MW reference turbine blade. They are calculated by curve fitting based on the results in Ren et al. (2018*b*).

Here, two domains are defined. The first domain, namely the control input domain, is the feasible region of the control inputs caused by the tension on the tugger lines, i.e.,

$$\mathbb{D}_c = \left\{ \boldsymbol{\tau} \in \mathbf{R}^2 | \boldsymbol{\tau} = \boldsymbol{B}\boldsymbol{f}, \boldsymbol{f} \in \mathbb{D}_f^3 \right\}. \tag{7}$$

Moreover, the required input domain, containing the required control input to compensate the wind-induced load acting on the blade, is defined by

$$\mathbb{D}_r = \{[F_{wx}(U_w), M_{wz}(U_w)]^\top | U_w \in \mathbb{D}_w = [U_{w,min}, U_{w,max}]\}, \quad (8)$$

where $U_{w,min}$ and $U_{w,max}$ are the minimum and maximum inflow speed. For a given mean wind speed and turbine class, the wind-induced loads can realistically be compensated by the control inputs from the tugger lines if $\mathbb{D}_r \subseteq \mathbb{D}_c$. In the following, a discussion is given about the placement of the connecting points of the tugger line on the yoke.

The control input domain $\mathbb{D}_c$ w.r.t. the placement of the third tugger line

The third tugger line is placed in the opposite direction relative to the other two tugger lines. The distance between its connecting point to the COG in the blade longitudinal axis is r_{t3}, e.g., $-10 \le r_{t3} \le 10$. A series of control input domain tests is conducted with parameter sweeps. The results are presented in Figs. 5-8.
Here are some summaries about $\mathbb{D}_c$:

- It is obvious that $\mathbb{D}_c$ for the three-tugger-line configuration is much broader than for a two-tugger-line arrangement.
- The shapes of $\mathbb{D}_c$ for the configuration with two-tugger-line configuration are rhombuses. While the shapes of $\mathbb{D}_c$ for three-tugger-lines configurations are hexagons.
- Typically, the choice of the two tugger lines are the line 1 and 2. From the proposed results, $\mathbb{D}_c$ is then small. The $\mathbb{D}_c$ for tugger line 1&3 and 2&3 are symmetric about the F_{tx}-axis. The farther the third tugger line is placed to the tugger line 1 or 2, the broader $\mathbb{D}_c$ can be achieved.
- $\mathbb{D}_c$ can be modified with the tugger line force input upper limitation f_{max}.

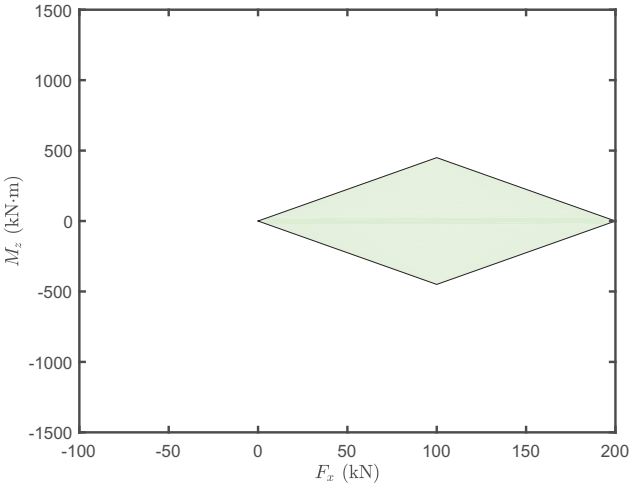

Fig. 5 Control domain with tugger line 1 and 2 ($f_1, f_2 \in [0, 100]$ kN and $f_3 = 0$).

The required input domain $\mathbb{D}_r$ w.r.t. mean-wind speeds and turbine classes

According to IEC (2005), the normal turbulence model (NTM) is given by

$$\sigma_1 = I_{ref}(0.75U_w + b),\ b = 5.6, \quad (9)$$

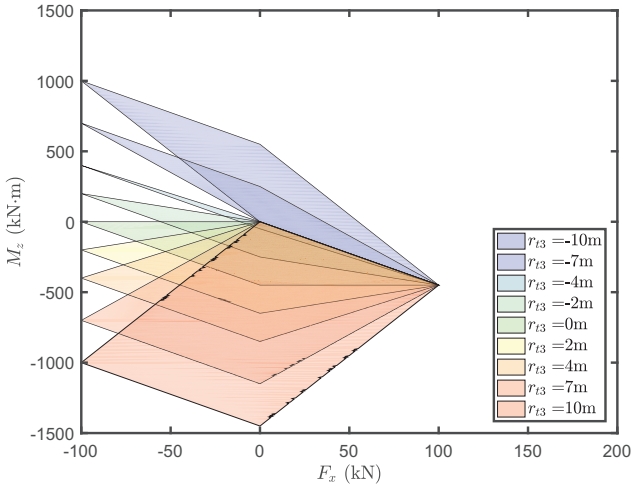

Fig. 6 Control domain with tugger line 1 and 3 ($f_1, f_3 \in [0, 100]$ kN and $f_2 = 0$).

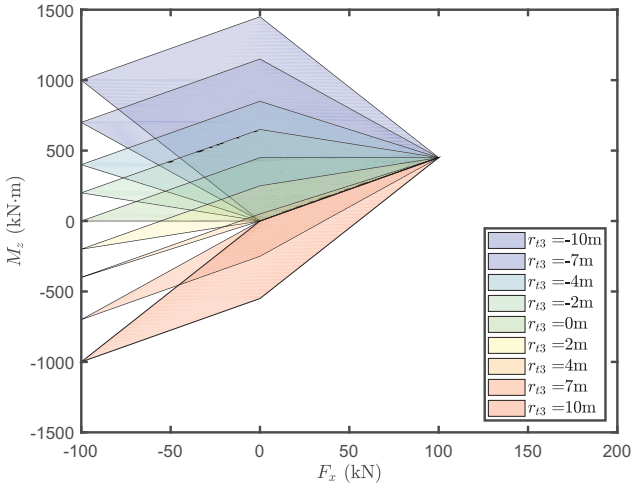

Fig. 7 Control domain with tugger line 2 and 3 ($f_2, f_3 \in [0, 100]$ kN and $f_1 = 0$).

where $I_{ref} = 0.16$ for wind turbine class A, $I_{ref} = 0.14$ for wind turbine class B, and $I_{ref} = 0.12$ for wind turbine class C. For a normal distribution, the possibility within the wind speed set $\mathbb{D}_w = \{U_w | \bar{U}_w - 3\sigma_1 \le U_w \le \bar{U}_w + 3\sigma_1\}$ is 99.8%. Therefore, the required control input can be calculated based on Eqn. (6), assuming that $U_w - 3\sigma_1$ and $U_w + 3\sigma_1$ are the lower and upper limits for the wind speed. The results are presented in Figs. 9-11.
Some results are summarized:

- For Class A wind turbine, $\mathbb{D}_r$ is broader than Class B, and they are both broader than Class C.
- Two-tugger-line scheme with tugger lines 1&2 is impossible to compensate the wind-induced loads without pretension.
- Two-tugger-line scheme with tugger lines 1&2 or 2&3 can compensate the wind-induced loads when the mean wind speed and turbulence intensity is limited in a range.
- Three-tugger-line configuration with the third tugger line con-

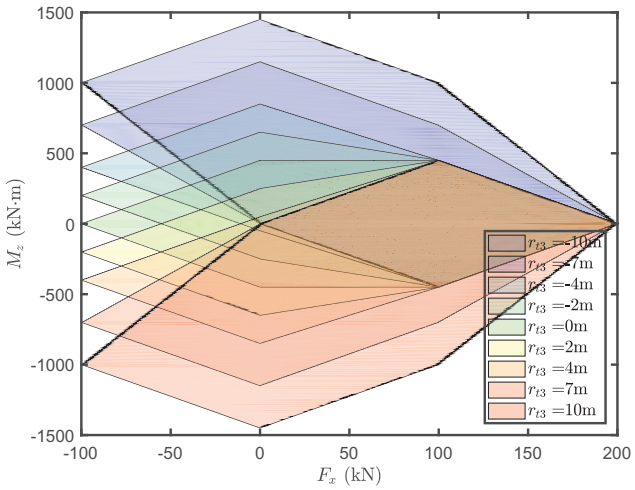

Fig. 8 Control domain with all three tugger lines ($f_1, f_2, f_3 \in [0, 100]$ kN).

nected to the yoke near the root is the best option for the proposed installation scenario.

In Ren et al. (2018*a*), tugger lines 1 and 2 are used. The pretension, which is needed to achieve negative control input, moves the control scope to the negative F_y direction. Therefore, the control performance is limited by the pretension. When the pretension is not enough and the wind-induced loads are so high that the force in tugger line 1 becomes 0, the system becomes unstable. In order to stabilize the blade without pretension, a three-tugger-line scheme is adopted in this paper.

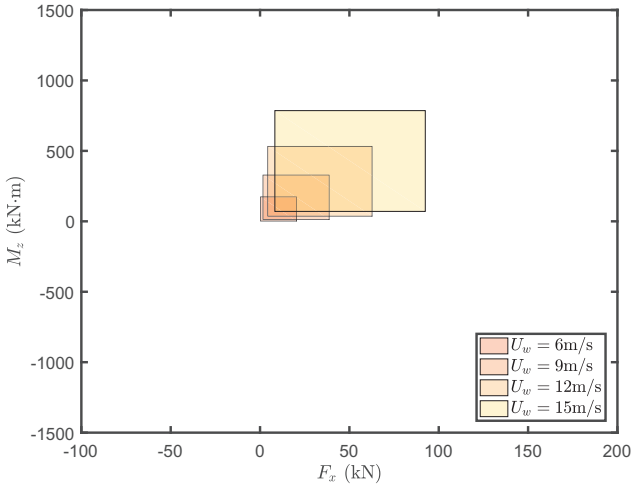

Fig. 9 Required input domain for class A turbulence.

Control allocation

As there are three force inputs (f_1, f_2, and f_3) and only two control inputs (F_{tx} and M_{tz}), the control allocation is an overdetermined problem. The problem is to find $\boldsymbol{f}_c$ from the desired $\boldsymbol{\tau}_c$, according to Eqn. (5). However, typical pseudoinverse, $\boldsymbol{f}_c = \boldsymbol{B}^\dagger \boldsymbol{\tau}_c$ with $\boldsymbol{B}^\dagger = (\boldsymbol{B}^\top \boldsymbol{B})^{-1}\boldsymbol{B}^\top$, is not applicable since there exists a constraint for each force input, i.e., $f_i \in \mathbb{D}_f, \forall i \in \{1, 2, 3\}$. In this paper, an online optimization solver is used

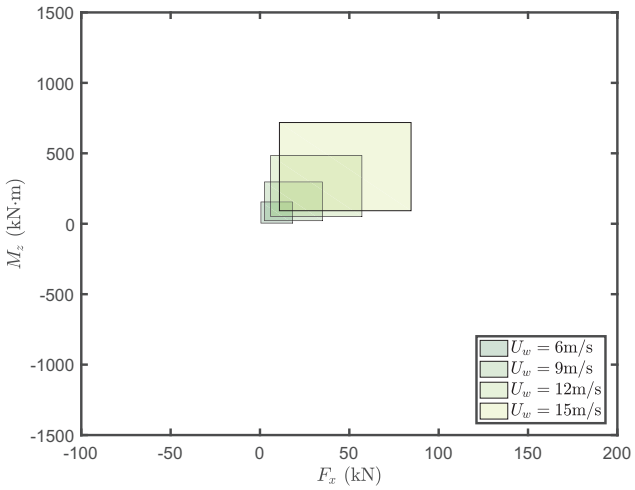

Fig. 10 Required input scope for class B turbulence.

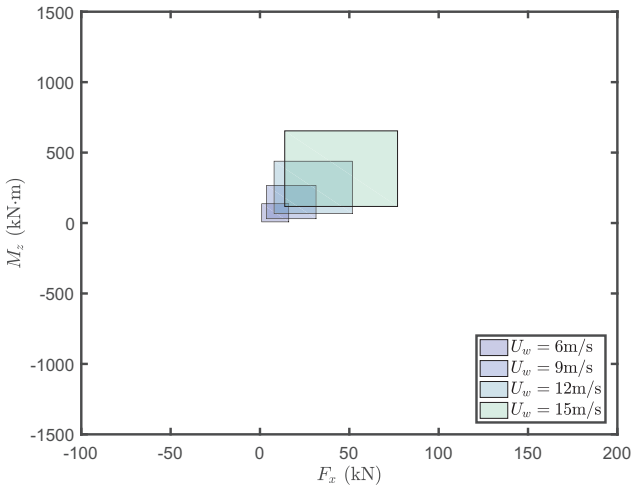

Fig. 11 Required input scope for class C turbulence.

to handle this constrained overdetermined control allocation problem. Because the computational conditions here is not high, the solver written in C language is fast enough to realize the online application. There are various programming solver to handle such programming problems. The CVXGEN is applied in this paper. CVXGEN is an online quadratic program optimization code generator (Mattingley & Boyd 2012).
The programming question is

$$\min_{\boldsymbol{f}_c} \left(\|\boldsymbol{B}\boldsymbol{f}_c - \boldsymbol{\tau}_c\|_{\boldsymbol{Q}_1} + \sum_i^{n_b} \|\boldsymbol{f}_c - \boldsymbol{\mathcal{F}}_i\|_{\boldsymbol{Q}_2} \right), \tag{10a}$$

subject to:
$$0 \le f_{c,1} \le f_{max,1}, \tag{10b}$$
$$0 \le f_{c,2} \le f_{max,2}, \tag{10c}$$
$$0 \le f_{c,3} \le f_{max,3}, \tag{10d}$$

where $\boldsymbol{Q}_1 \in \mathbb{R}^{2\times2}$ and $\boldsymbol{Q}_2 \in \mathbb{R}^{3\times3}$ are the weighting matrices in the objective function, $\boldsymbol{\mathcal{F}} \in \mathbb{R}^{3\times n_b}$ is a buffer matrix to store the previous data which $\boldsymbol{\mathcal{F}}$ updates for each time instant after finding the optimal solution $\boldsymbol{f}_c^*$ of Eqn. (10), $\boldsymbol{\mathcal{F}}_i$ is the i^{th} column of $\boldsymbol{\mathcal{F}}$, and n_b is the number of buffer-stored time instants.

The update law is given by

$$\mathcal{F} = [\mathcal{F}_{2:n_b}, \boldsymbol{f}_c^*], \tag{11}$$

where $\mathcal{F}_{2:n_b}$ contains the $n_b - 1$ newest columns of matrix the $\mathcal{F}$. The aim to introduce matrix $\mathcal{F}$ is to avoid sudden change and ensure smooth trajectories of the commanded tension force $f_{c,i}$. The values of the diagonal elements in $\boldsymbol{Q}_2$ should be much smaller than those in $\boldsymbol{Q}_1$ in case of slowing down the tension update.

Actuator dynamics

In reality, whether the desired tugger line forces can be supplied in time depends on the actuator characteristics. Due to the physical limitations of the actuators, the control signals cannot reach any desired values or at any desired rate. In this study, the actuator dynamics is simplified as a stable first-order dynamics, which can be expressed in the frequency domain by the transfer function

$$\frac{f_i(s)}{f_{c,i}(s)} = \frac{1}{T_{fi}s + 1},\ i \in \{1, 2, 3\}, \tag{12}$$

where T_{fi} is the time constant of the lowpass filter, $f_{c,i}$ denotes the control input command signal from the proposed controller and allocation algorithm, i.e., $\boldsymbol{f}_c$, and f_i is the actual physical tugger line force applied to the system at a specific time.
A discrete form of this lowpass filter in time domain is

$$f_i(t_k) = (1 - a_i)f_i(t_{k-1}) + a_i f_{c,i}(t_k),\ i \in \{1, 2, 3\}, \tag{13}$$

where t_k is the time at the k^{th} sample instants with a fixed sampling interval h and $a_i = h/(T_{fi} + h)$.

SIMULATION

Overview

Numerical simulations are conducted in HAWC2 using MATLAB/Simulink to control the external force inputs. Selected properties of the blade installation model and the controller parameters are summarized in Table 1. The blade of the NREL 5 MW reference wind turbine is used (Jonkman et al. 2009).
The simulation environmental parameters are selected as a Class C turbine with a mean wind speed $U_w = 12$ m/s, and the turbulence intensity (TI) are calculated according to IEC (2005). The turbulence is simulated with Mann's turbulence model. Each simulation lasted 1000 seconds. In the response statistics, the first 400 seconds are removed during postprocessing to avoid the start-up transient effect.
We select the mean wave direction the same as the mean wind direction, with the significant wave height 2 m and wave period $T_p = 6$ s. For a given pair of H_s and T_p, the wave angle of attack is selected as the most critical angle, where the hub motion in the wind inflow direction is the largest.
The criteria are the absolute/relative blade root center's motion radius (Jiang et al. 2018), which is defined by the square root of the sum of motion in vertical and flow-wise direction. The absolute blade root center's motion radius η_{r0} and the relative blade root center's motion radius η_{rh} are defined by

$$\eta_{r0}(t) = \sqrt{(x_r(t) - \bar{x}_r)^2 + (z_r(t) - \bar{z}_r)^2}, \tag{14a}$$

$$\eta_{rh}(t) = \sqrt{(x_r(t) - x_h(t) - \bar{x}_r + \bar{x}_h)^2 + (z_r(t) - z_h(t) - \bar{z}_r + \bar{z}_h)^2}, \tag{14b}$$

where x_r, z_r, x_h, and z_h define the positions of blade root center and hub center, respectively.
CVXGEN is used for the control allocation to calculate the control input on each tugger lines $\boldsymbol{f}_c$ based on the desired system input $\boldsymbol{\tau}_c$. C++ codes are generated with an online interface, which ensures a fast computational speed. The calculation speed satisfies a real-time online optimization scenario.

Time domain simulation results

The time domain simulation results are presented in Figs. 13-16. The tension in tugger line 2 and 3 is much smaller compared to the passive installation approach, while the tension in tugger line 1 increases. It is noticed that the blade's motion is greatly reduced by the proposed PID controller. The motion radii of the active-control scheme is limited within a smaller range than the typical passive method. With a 100 Hz sampling frequency, the accumulated errors for the active scheme is much smaller than the passive configuration. The blade's motion in the inflow direction is also greatly reduced. Therefore, the proposed controller can reduce the blade's relative motion to the hub. The achieved total load from command signals $\boldsymbol{B}\boldsymbol{f}_c$ follows the desired values $\boldsymbol{\tau}_c$ well. Furthermore, the tension on each wire rope stays within a reasonable range with a limited rate of change. Thus, the control allocation module works well.

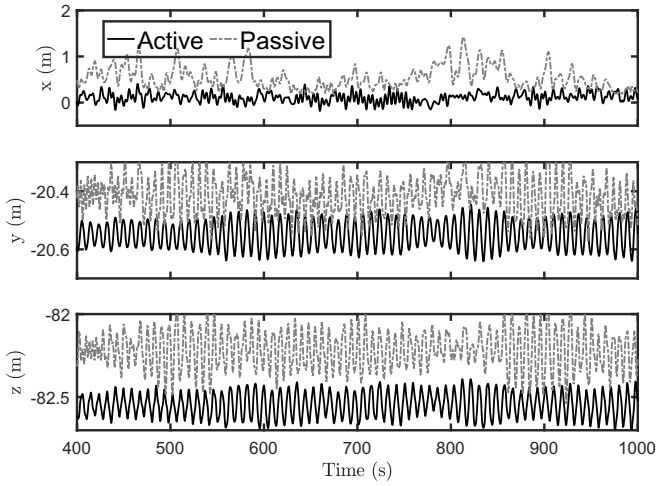

Fig. 12 Position of the blade root center, $U_w = 12$ m/s, $TI = 0.146$, $H_s = 2$ m, and $T_p = 6$ s.

CONCLUSION AND FUTURE RESEARCHES

This paper proposes a closed-loop scheme for tugger line force control for single blade installation. A PID controller is adopted to insert restoring, damping, and integral forces to the blade dynamics in the mean wind direction and the moment about the vertical axis. The placement of tugger lines are discussed, where it was shown that a 3^{rd} well-located tugger line increases the control space significantly. The control allocation is achieved with a convex programming solver. To verify the performance of the controller, time-domain simulations are conducted in turbulent wind conditions using MATLAB and HAWC2. Motion radii are employed as the criteria to evaluate the controller's performance. The proposed active control scheme can stabilize the blade in turbulence wind. The active scheme has a superior performance over the passive scheme.
In future work, other scenarios of single blade installation will be addressed. For example, flexibility of the crane tip should be considered for the boundary condition of the lift wire. Furthermore, the spanwise motion should also be canceled by the controller.

Table 1 Parameters used for numerical simulations.

Parameters	**Unit**	**Value**
Mean wind speed	m/s	12
Turbulence intensity factor	-	0.146 (IEC Class C)
Water depth	m	30
Monopile foundation length	m	36
Monopile sub-structure length	m	30
tower length	m	77.6
Position of the crane tip	m	$[0, 0, -110]^\top$
Yoke mass m_y	ton	20
Blade mass m_b	ton	17.74
Blade moment of inertia about COG I_b	kg·m^2	4.31e6
Blade length	m	62.5
Arms of the tugger line forces $[r_{t1}, r_{t2}, r_{t3}]$	m	[-4.5,4.5,-6.22]
Length of lift wire	m	9.2
Stiffness of lift wire	N/m	5.59e8
Length of slings	m	9.0
Stiffness of slings	N/m	1e8
Lift wire and spring damping ratio	-	1%
Gain matrix of P controller $\boldsymbol{K}_p$	-	diag{1e5,1e7}
Gain matrix of D controller $\boldsymbol{K}_d$	-	diag{1e4,0.5e6}
Gain matrix of I controller $\boldsymbol{K}_i$	-	diag{1e3,3e5}
Weighting matrix $\boldsymbol{Q}_1$	-	diag{100,1}
Weighting matrix $\boldsymbol{Q}_2$	-	diag{1e-7,1e-7,1e-7}

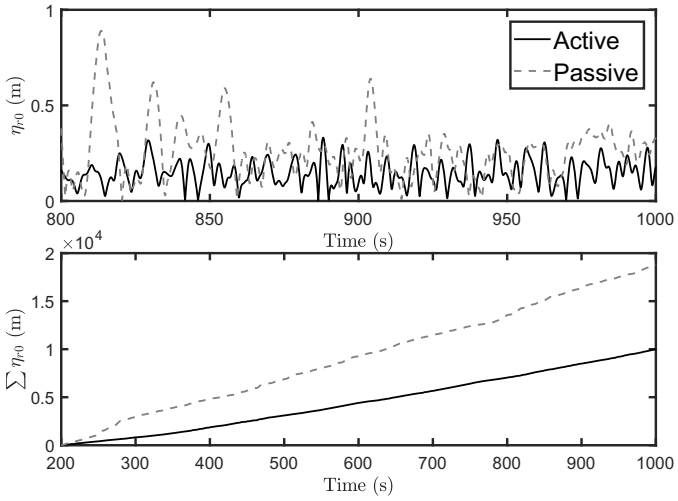

Fig. 13 Absolute motion radius history of the blade root center η_{r0} and accumulated error of the motion, U_w = 12 m/s, TI = 0.146, H_s = 2 m, and T_p = 6 s.

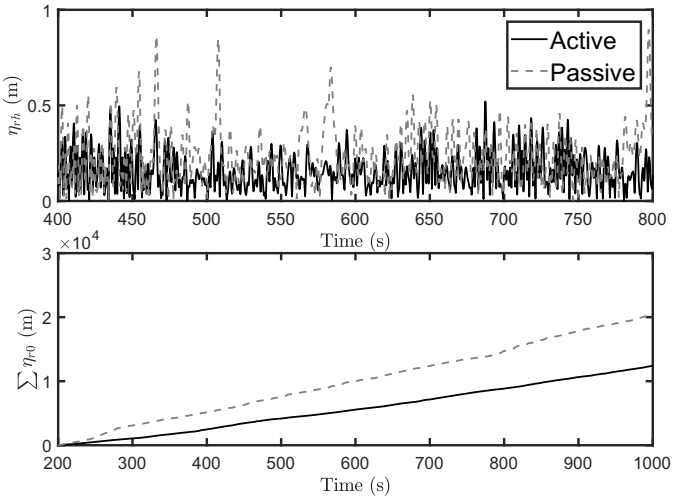

Fig. 14 Relative motion radius history between the hub and blade root center and accumulated error of the motion η_{rh}, U_w = 12 m/s, TI = 0.146, H_s = 2 m, and T_p = 6 s.

ACKNOWLEDGMENT

This work was supported by the Research Council of Norway (RCN) through the Centre for Research-based Innovation on Marine Operations (CRI MOVE, RCN-project 237929), and partly by the Centre of Excellence NTNU AMOS (RCN-project 223254).

REFERENCES

American Petroleum Institute (2000), *API RP 2A-WSD Recommended Practice for Planning, Designing and Constructing Fixed*

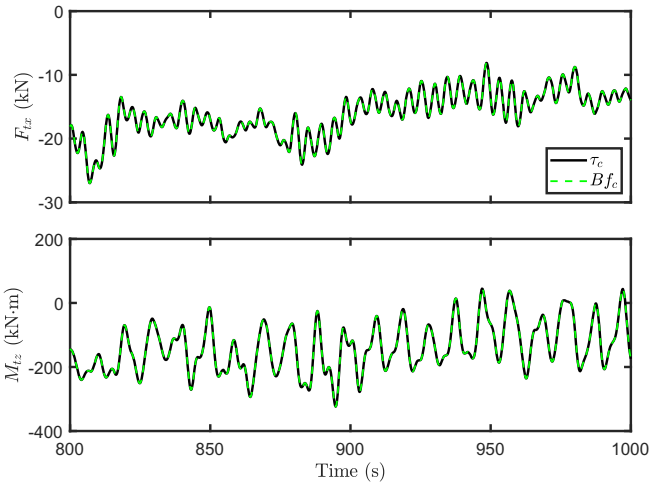

Fig. 15 Performance to track the desired control input $\boldsymbol{\tau}_c$ and $\boldsymbol{Bf}_c$, U_w = 12 m/s, TI = 0.146, H_s = 2 m, and T_p = 6 s.

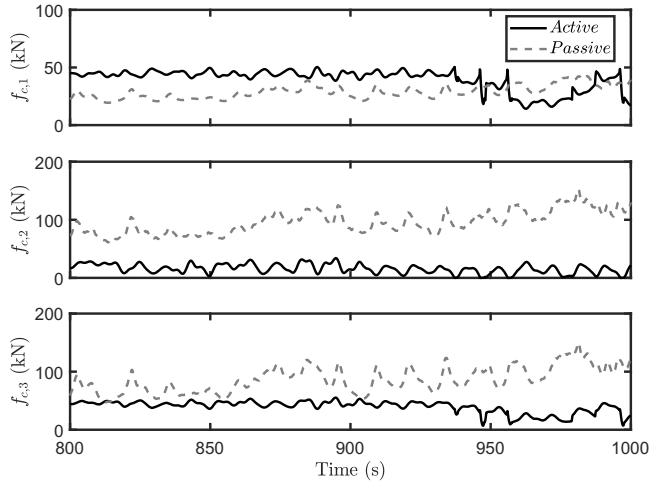

Fig. 16 History of the tension on tugger lines $\boldsymbol{f}_c$, U_w = 12 m/s, TI = 0.146, H_s = 2 m, and T_p = 6 s.

Offshore Platforms: Working Stress Design, American Petroleum Institute.
URL: *https://books.google.no/books?id=FgwfnQEACAAJ*

Arany, L., Bhattacharya, S., Macdonald, J. H. & Hogan, S. J. (2016), 'Closed form solution of eigen frequency of monopile supported offshore wind turbines in deeper waters incorporating stiffness of substructure and ssi', *Soil Dynamics and Earthquake Engineering* **83**, 18–32.

Bhattacharya, S. & Adhikari, S. (2011), 'Experimental validation of soil–structure interaction of offshore wind turbines', *Soil Dynamics and Earthquake Engineering* **31**(5), 805–816.

DNV (2000), *Environmental conditions and environmental loads*, Det Norske Veritas.

Gaunaa, M., Bergami, L., Guntur, S. & Zahle, F. (2014), 'First-order aerodynamic and aeroelastic behavior of a single-blade installation setup', *Journal of Physics: Conference Series* **524**(1), 012073.

Gaunaa, M., Heinz, J. & Skrzypiński, W. (2016), 'Toward an engineering model for the aerodynamic forces acting on wind turbine blades in quasisteady standstill and blade installation situations', *Journal of Physics: Conference Series* **753**(2), 022007.

HighWind (n.d.), 'The boom lock', `http://www.high-wind.eu/boomlock/`. [Online; accessed 10-August-2017].

IEC (2005), Wind turbine generator systems-part 1: Safety requirements, Standard, International Electrotechnical Commission, Geneva, Switzerland.

Jiang, Z., Gao, Z., Ren, Z., Li, Y. & Duan, L. (2018), 'A parametric study on the blade mating process for monopile wind turbine installations under rough environmental conditions', *Engineering Structures under review* .

Jonkman, J., Butterfield, S., Musial, W. & Scott, G. (2009), 'Definition of a 5-mw reference wind turbine for offshore system development', *National Renewable Energy Laboratory, Golden, CO, Technical Report No. NREL/TP-500-38060* .

Jonkman, J., Butterfield, S., Passon, P., Larsen, T., Camp, T., Nichols, J., Azcona, J. & Martinez, A. (2008), Offshore code comparison collaboration within iea wind annex xxiii: phase ii results regarding monopile foundation modeling, Technical report, National Renewable Energy Laboratory (NREL), Golden, CO.

Kuijken, L. (2015), Single blade installation for large wind turbines in extreme wind conditions, Master's thesis, Technical University of Denmark & TU Delft.

Liftra (n.d.), 'LT575 blade dragon', `http://liftra.com/product/blade-dragon/`. [Online; accessed 10-August-2017].

Mann, J. (1998), 'Wind field simulation', *Probabilistic Engineering Mechanics* **13**(4), 269 – 282.

Mattingley, J. & Boyd, S. (2012), 'Cvxgen: A code generator for embedded convex optimization', *Optimization and Engineering* **13**(1), 1–27.

Moné, C., Hand, M., Bolinger, M., Rand, J., Heimiller, D. & Ho, J. (2017), 2015 cost of wind energy review, Technical report, National Renewable Energy Laboratory.

Ren, Z., Jiang, Z., Skjetne, R. & Gao, Z. (2018*a*), 'An active tugger line force control method for single blade installations', *Wind Energy* . under review.

Ren, Z., Jiang, Z., Skjetne, R. & Gao, Z. (2018*b*), 'Development and application of a simulator for offshore wind turbine blades installation', *Ocean Engineering* . under review.

Schneider, H. (2014), 'Single blade installation takes the lead'. [Online; accessed 3-October-2017].
URL: *`http://a2seanews.editionmanager.com/2014/04/04/single-blade-installation-takes-the-lead/`*

Verma, A. S., Vedvik, N. P. & Gao, Z. (2017), Numerical assessment of wind turbine blade damage due to contact/impact with tower during installation, Vol. 276, p. 012025.

Zhao, Y., Cheng, Z., Sandvik, P. C., Gao, Z. & Moan, T. (2018), 'An integrated dynamic analysis method for simulating installation of a single blade for offshore wind turbines', *Ocean engineering* . under review.